Porous Silicon Templates for Superconducting Devices

Carmine Attanasio and Serghej L. Prischepa

Contents

Abstract

The use of porous silicon (PS) templates in the field of superconducting nanoelectronics is reviewed. We focus on the influence of the morphology of the pores (porosity, average pore diameter) on the superconducting properties of ultrathin films deposited on these templates. We describe and discuss some basic and advanced properties of the obtained nanostructured superconductors. In particular, we show that, due to the extremely reduced dimensions of PS templates, the formation of commensurate vortex structures can be realized at low temperatures and at matching fields as high as $\mu_0 H_1 \approx 1$ T. We also show that with this fabrication procedure, we can obtain networks of one-dimensional superconducting nanowires, which exhibit features typical of quantum phase slip (QPS) phenomena. This creates preconditions for the development and implementation of new highly sensitive radiation detectors, magnetometers, QPS qubits, QPS transistors, and quantum current standards.

C. Attanasio
Università degli Studi di Salerno, Fisciano, Italy
e-mail: attanasio@sa.infn.it

S.L. Prischepa (✉)
Department of Telecommunications, Belarusian State University of Informatics and Radioelectronics, Minsk, Belarus
e-mail: prischepa@bsuir.by

L. Canham (ed.), *Handbook of Porous Silicon*,
DOI 10.1007/978-3-319-04508-5_106-1

Keywords
Porous silicon template • Ultrathin superconducting film • Matching effect • Nanowire network • Thermal fluctuations • Quantum tunneling

Introduction

A variety of fascinating phenomena has been reported when a thin film of a type II superconductor is grown on an ordered array of artificial pinning centers (antidots) with dimension of the order of the vortex core. (Readers who are not familiar with the phenomenon of superconductivity are recommended to read the textbook by Schmidt (1997).) Strong enhancement in the magnetization curves, $M(H)$ (Welp et al. 2002), in the dependence of critical current density, J_c, and on the external magnetic field, H (Moshchalkov et al. 1998), and anomalies in the (H,T) phase diagram (Prischepa et al. 1994; Welp et al. 2002; Trezza et al. 2008) have been observed when the matching conditions, $H = nH_1$, are fulfilled. Here, n is an integer, and H_1 is the value of the magnetic field at which the vortex lattice spacing is equal to the period of the array of defects, a. In the case of a triangular array, $H_1 = 2\Phi_0/\sqrt{3}a$, where Φ_0 is the flux quantum. It follows that the shorter the period of the antidots, the higher the matching fields at which the vortex confinement can be realized. If the artificial structure of defects is created by means of a lithographic process, the values of the matching fields are typically in the range of a few Oersteds. For this reason, matching effects are observed only for temperatures very close to the critical temperature T_c, typically at $t = T/T_c \geq 0.95$. In order to both increase the matching field and decrease the temperature where the effect is present, the period of the pinning structure should be reduced to less than 100 nm, which implies a value for H_1 higher than 1 T. A good method to achieve this goal is to use self-assembled templates with characteristic features in the nanometric scale (Xia et al. 1999). Historically, the first templates used for such kind of nanopatterning (i.e., when the superconducting thin film is deposited *onto* a porous template) were porous anodic alumina Al_2O_3 substrates (Prischepa et al. 1994; Welp et al. 2002; Vinckx et al. 2007) in which the pore diameter was in the range 25–200 nm, while the porosity was around 50 %. With these systems, matching fields of thousands of Oersteds were obtained.

Porous silicon (PS) is an even more promising self-assembled template for superconductors because silicon is very usefully used as a substrate for the deposition of refractory superconductors, such as Nb and NbN that currently are most widely utilized in superconducting electronics. PS is constituted by a network of pores distributed in nanocrystalline silicon matrix (Bisi et al. 2000), and it is a material that offers a considerable technological interest in different fields (Cunin 2014). The possibility of changing the porosity of PS up to high values leads to another unique opportunity, namely, to the use of PS templates to create one-dimensional (1D) superconductors and/or networks of 1D superconducting channels or nanowires (NW). 1D superconductivity occurs when the width of the

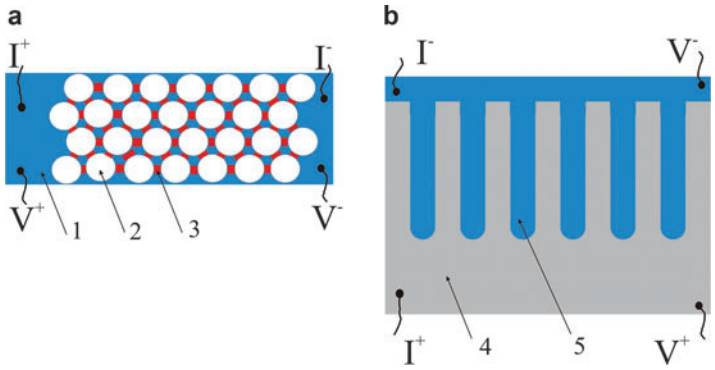

Fig. 1 Schematic sketch of the geometry of a NW network when the superconducting film deposited (**a**) *onto* and (**b**) *inside* the pores of a porous template. *1* superconducting film, *2* pore, *3* nanowire (restriction), *4* porous template, *5* superconducting nanowire inside the pore. Configurations for the current supply and voltage drop measurement are also shown

superconducting strip deposited between the pores becomes equal or smaller than the superconducting coherence length, ξ. However, a network of superconducting NWs can be obtained also by electrodepositing a superconductor *inside* the pores (Ogata and Fukami 2014). As a matter of fact, porous glasses were the first templates used for the growth of superconducting NWs of In, Pb, Sn, Ga, and BiPb *inside* pores (Graf et al. 1992; Bogomolov et al. 1993; Charnaya et al. 1998). These two different morphologies of networks of superconducting NWs are schematically drawn in Fig. 1.

Both thermal-activated phase slip (TAPS) and quantum phase slip (QPS) processes dominate the behavior of 1D superconductors (Giordano 1990) independently on whether the superconducting NWs are formed *onto* or *inside* pores. These dissipation processes cause the nanowires to remain resistive much below the superconducting transition temperature. Multiply connected nanowire arrays may be the core of superconducting devices working as magnetometers and radiation detectors (Hopkins et al. 2005). Recently, the proposed duality between Josephson junctions and QPS effects (Mooij and Nazarov 2006) strengthened the interest in these low-dimensional systems, which, under appropriate conditions, could show coherent QPS-related phenomena (Astafiev et al. 2012). This evidence could lead to the realization of QPS qubits (Mooij and Harmans 2005), QPS transistors (Hongisto and Zorin 2012), and quantum current standards (Webster et al. 2013). Therefore, the approach to NWs fabrication became in itself a research field, spanning from ion-beam design (Tettamanzi et al. 2009), to molecular templating (Remeika and Bezryadin 2005), and deposition inside (Tian et al. 2005) or on top (Luo et al. 2012) of nanoporous self-assembled templates. In particular, the latter method is especially appealing since it allows the fabrication of patterned nanostructures in a single step, rapidly, cheaply, and with reproducibility achieved on a large-scale area. Therefore, for the application in superconducting electronics, the following important

parameters of PS can be relevant – the average diameter of pores ∅, the porosity P (which determines the average interpore distance, Λ), and the quality of the silicon surface between pores which determines the properties of the deposited superconducting film. In fact, if it would contaminate the superconductor, the template could not be successfully used to realize any superconducting device. The diameter of the pores can be easily changed from micrometers to nanometers by using substrates of appropriate doping and different regimes of anodization. The porosity depends on the parameters used during the electrochemical process, and it can be adjusted to lie in the range 0.2–0.8.

In the following, we mainly review the use of PS as a template for the growth of nanoperforated superconducting Nb films. The reduced dimensions of a PS template result in the formation of commensurate vortex structures at matching fields as high as $\mu_0 H_1 \approx 1$ T. We also show that networks of 1D superconducting nanowires exhibit features typical of QPS phenomena.

Matching Effects

PS layers were fabricated by standard electrochemical etching of *n*-type single crystalline Si:Sb, 0.01 Ω × cm, in 48 % water solution of HF. The variation of the anodization current in the range 20–100 mA/cm^2 results in the change of the porosity of the PS within the range from 35 % to 85 %, as shown in Fig. 2. After a superconducting film is deposited on the template, this range of porosity allows to obtain dimensions which are useful for chip-on applications. Nowadays, a porosity as high as 95 % can be reached by supercritical drying. The light exposition by 100 W tungsten lamp allowed to change the average pore diameter. The anodization time was chosen in the range 0.5–4 min in order to get porous layers with a thickness ranging from 0.5 to 4 μm. The nominal pore diameter was ∅ = 10–15 nm, and the average distance between pores was estimated as Λ = 15–20 nm for light-exposed templates and Λ = 40 nm for samples obtained without illumination.

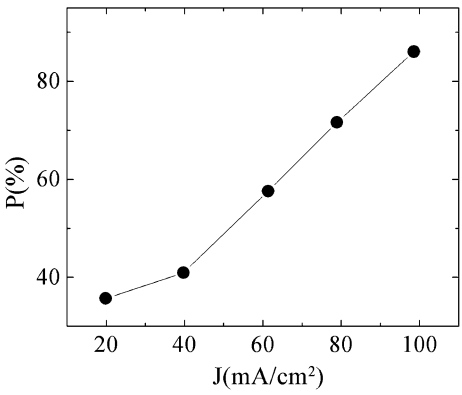

Fig. 2 Dependence of the porosity of the *n*-type PS on the anodization current

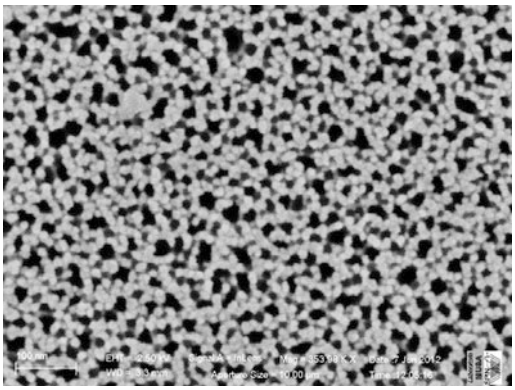

Fig. 3 Morphology of a thin Nb film ($d_{Nb} = 3.5$ nm) deposited onto a PS template with $\varnothing = 15$ nm and $\Lambda = 50$ nm

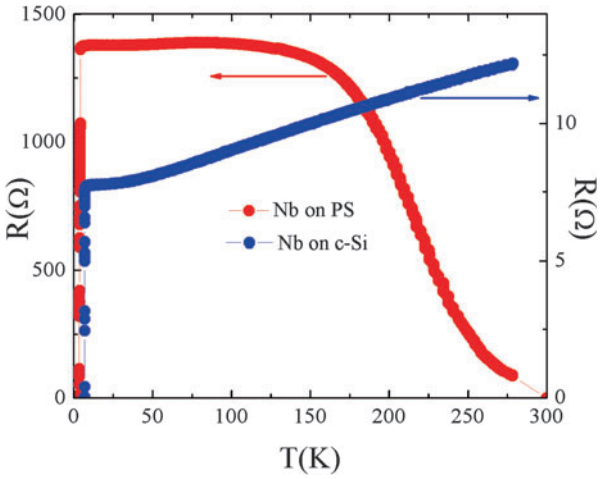

Fig. 4 $R(T)$ dependence for a Nb thin film deposited on a PS template (*red curve*, left scale) and on a c-Si substrate (*blue curve*, right scale)

Nb thin films were grown on the top of PS templates in a UHV dc diode magnetron sputtering system with a base pressure 10^{-8} mbar and sputtering Argon pressure of 10^{-3} mbar. The typical rate of Nb deposition was 0.3 nm/s controlled by a quartz crystal monitor. Since the effect of the periodic template would be reduced when the Nb thickness, d_{Nb}, exceeds the pore diameter $\varnothing$ (Cirillo et al. 2012), the value of d_{Nb} was kept below 15 nm. In Fig. 3 we show the morphology of a Nb film deposited onto a PS template: d_{Nb} was equal to 3.5 nm, $\varnothing$ to 15 nm, and Λ to 50 nm. It should be noted that the surface roughness of the template would play a significant role on the quality of the deposited Nb film. This issue is still under investigation.

The PS template has a significant impact on the transport properties of the Nb film. In Fig. 4 we show the resistance R versus temperature T dependence for a Nb film ($d_{Nb} = 8.5$ nm) deposited on a PS template ($\varnothing = 15$ nm, $\Lambda = 40$ nm) and on a c-Si substrate ($d_{Nb} = 15$ nm). We see that the PS template influences both the

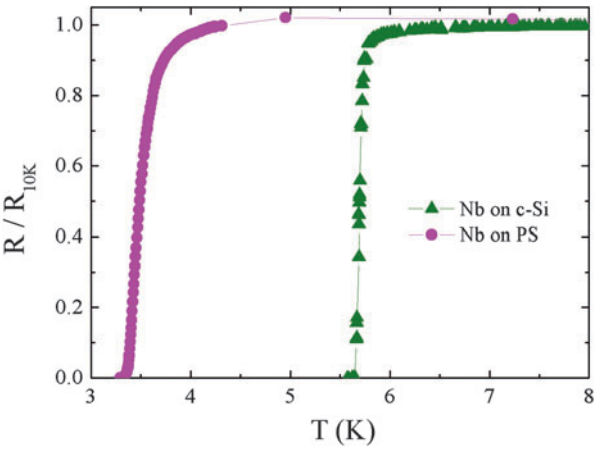

Fig. 5 The low-temperature part of the $R(T)$ dependence for a Nb thin film deposited on a PS template (*purple circles*) and on a c-Si substrate (*green triangles*)

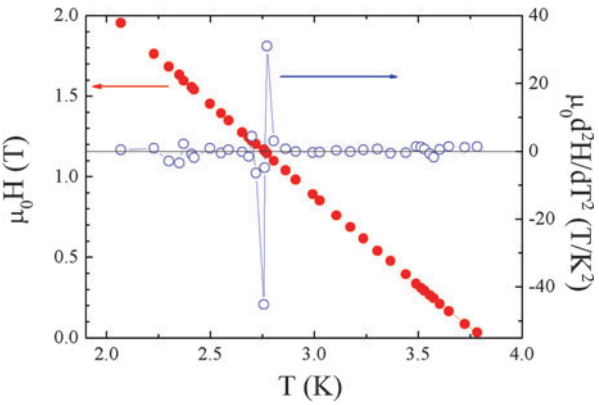

Fig. 6 Left scale: $H_{c2\perp}$ versus T for the Nb thin film ($d_{Nb} = 8.5$ nm) grown on the PS template ($\varnothing = 15$ nm, $\Lambda = 40$ nm). Right scale: $dH_{c2\perp}{}^2/dT^2$ versus T

absolute value of the resistance and the overall $R(T)$ behavior that, at high temperatures, becomes more semiconducting-like. However, as it is evident from Fig. 5, where the low-temperature region of the $R(T)$ dependence is plotted for both samples, the Nb film deposited on the PS template is still superconductor, with $T_c = 3.5$ K. In Fig. 6 we show the (H,T) phase diagram of the same Nb thin film deposited on the PS template. The magnetic field was applied perpendicular to the surface. The $H_{c2\perp}(T)$ dependence presents some peculiarities, which indicate that the superconducting properties are influenced by the introduction of the porous array. If we plot the second derivative $d^2H_{c2\perp}/dT^2$ versus the temperature, we can see that its sign changes from positive to negative at $\mu_0 H \approx 1.16$ T. This value is very close to the nominal first matching field that we expect for this PS template, namely, $\mu_0 H_1 \approx 1.30$ T. On the other hand, the $H_{c2\perp}(T)$ dependence of Nb film deposited on c-Si substrate does not reveal such peculiarities (Trezza et al. 2009).

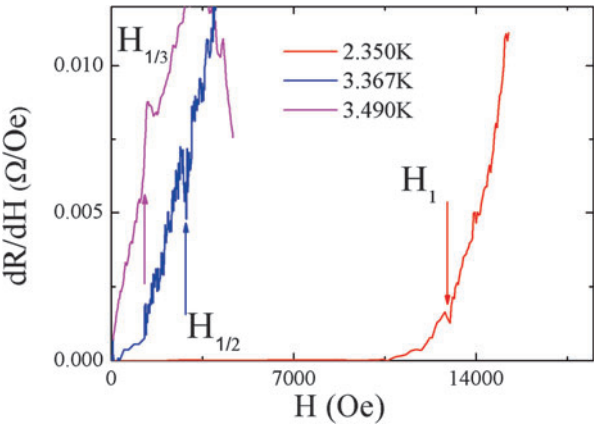

Fig. 7 dR/dH as a function of the applied magnetic field for different T for the Nb thin film ($d_{Nb} = 8.5$ nm) grown on the PS template ($\varnothing = 15$ nm, $\Lambda = 40$ nm). The *arrows* indicate the field where a bump is present in each curve

From the value of H_1, it follows that the period of the porous template, which affects the superconducting properties of the Nb thin film, is $a_0 = 42$ nm. From the result of Fig. 6, it is also possible to evaluate the value of superconducting coherence length at zero temperature, which is $\xi_0 = 9.1$ nm. This means that each pore traps only one fluxon so that the regime of individual pinning dominates in this sample (Moshchalkov et al. 1998).

The study of the $R(H)$ curves allows a better understanding of possible matching scenarios in nanoperforated Nb thin films. In Fig. 7 we show the first derivative, dR/dH, as a function of the applied magnetic field for different temperatures for the same Nb thin film. We see that small local maxima are present at specific values of the magnetic field. For the sample deposited onto c-Si substrate, these features are absent (Trezza et al. 2009). The bumps in the first derivative reflect the presence of a small dip in the corresponding $R(H)$ curves at the same value of the magnetic field. This effect is related to pinning enhancement when the period of the vortex structure is commensurate with the period of the pores (Patel et al. 2007). The bumps in the dR/dH appear at values of H for which the magnetic field threading each unit cell is equal to the flux quantum, Φ_0. In Fig. 7 this peculiarity in the dR/dH behavior is observed at $\mu_0 H_{bump} \approx 0.126$ T for 3.490 K. The period of the vortex lattice at this field is $a = 128$ nm, i.e., about three times the interpore spacing of this sample, $a_0 = 42$ nm. The result shown in Fig. 7 for $T = 3.367$ K corresponds to twice the interpore distance (at $T = 2.350$ K this simply corresponds to the interpore spacing). In Fig. 8 we show the position of bumps measured at different T. By solid lines, we plot the first matching field H_1 and fractional fields that correspond to double, triple, and quaternary periods ($H_{1/2}$, $H_{1/3}$, and $H_{1/4}$, respectively). The dashed vertical lines locate the range in which each matching field could be observed because of a statistical distribution of the interpore distance (Trezza et al. 2008). The result of Fig. 8 tells that the coherence in the vortex lattice induced by the PS template is propagated up to distance of 170 nm.

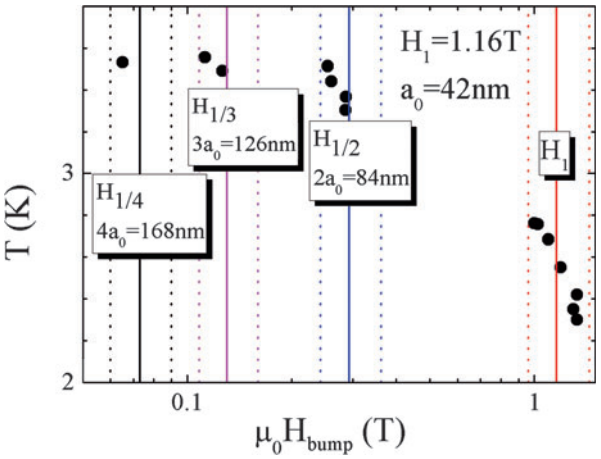

Fig. 8 Points of coordinates T-H_{bumps} identify the values of fields at which bumps were observed in the dR/dH curves at fixed T. The *solid lines* correspond to the different matching fields achieved with the interpore spacing $a_0 = 42$ nm. The *dotted lines* are obtained forasmuch as the regularity of the interpore distance is achieved within the 10 % of the average distance

Nanowire Networks

The formation of interconnected networks consisting of Nb ultrathin superconducting nanowires can be achieved by using PS as a template. The extremely reduced film thickness favors the deposited material to occupy only the substrate pitch; therefore, the as-sputtered films result as a network of interconnected wires, whose average width, w, can be assumed to be equal to the periodic pore spacing minus the pore diameter (see, e.g., Fig. 3). Because w is of the order of nanometers, it is comparable to the superconducting coherence length, ξ, and hence each individual wire behaves as a 1D object. Therefore, the whole samples show broadened resistive transitions, which can be described by theoretical models which take into account both thermal and quantum fluctuations of the superconducting order parameter in 1D superconductors (Golubev and Zaikin 2008).

PS templates with an average pore diameter $\varnothing \approx 10$–20 nm and an average interpore spacing $\Lambda \approx 20$–50 nm have been used for this investigation. FESEM analyses revealed that the optimal Nb thickness to investigate superconducting properties of the NW array should be in the range $d_{Nb} \approx 9$–12 nm. This assures that the wires are continuous, while preserving the presence of a well-defined network (Cirillo et al. 2012). With this approach, the PS template guides the formation of an array of interconnected Nb nanowires (NWs), the single wire width being equal to the substrate pitch ($w \approx 10$–35 nm). Moreover, the Nb films were patterned both by optical and electron beam lithography to create a strip configuration. When the optical lithography was used, the obtained dimensions were $W_b \approx 10$, 20 μm for the width and $L_b = 100$ μm for the length (Cirillo et al. 2012). The use of electron beam lithography gave the possibility to reduce significantly the width of the microstrip to $W_b \approx 1.67$ μm, while the length was chosen to be $L_b = 30$ μm (Trezza et al. 2013). As a consequence, a different number, N, of interconnected NWs was obtained: $N \approx 250$–500 ($N \approx 30$) for samples fabricated

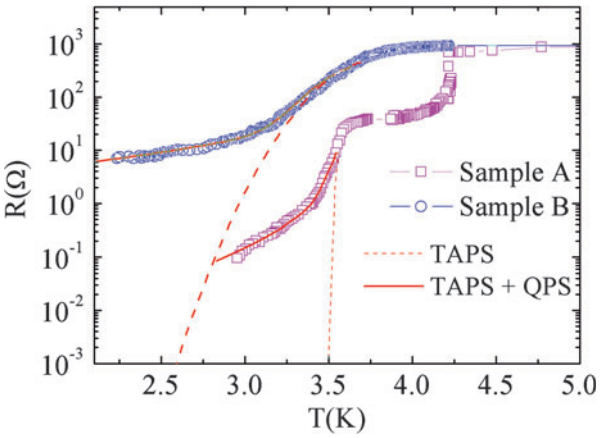

Fig. 9 Resistive transitions, $R(T)$, of two Nb nanowire networks. *Squares* represent data for sample A patterned by optical lithography. *Circles* are for sample B patterned by electron beam lithography. The *solid red lines* are the theoretical curves including both TAPS and QPS contributions, Eq. 1. The *dashed red lines* are the results of the fitting procedure including only TAPS contribution in Eq. 1

using optical (Cirillo et al. 2012) [electron beam (Trezza et al. 2013)] lithography. The resistive transitions to the superconducting state, $R(T)$, for two samples patterned by optical lithography (sample A, $N \approx 500$) and by electron beam lithography (sample B, $N \approx 30$) are presented in Fig. 9. The normal state resistance R_n, d_{Nb}, and w_b were almost the same for both samples, $R_n \approx 10\ \Omega$, $d_{Nb} = 12$ nm, and $w_b \approx 20$–30 nm. The experimental data were fitted to the expression (Lau et al. 2001)

$$R(T) = \left[R_n^{-1} + \left(R_{TAPS} + R_{QPS}\right)^{-1}\right]^{-1}, \tag{1}$$

where R_{TAPS} and R_{QPS} represent the contribution to the resistance due to thermal activation and quantum tunneling of phase slips, respectively. $R_{TAPS} \sim \sqrt{F(T)/k_B T}\exp[-F(T)/k_B T]$ (Golubev and Zaikin 2008) and, with exponential accuracy (Golubev and Zaikin 2001; Lehtinen et al. 2012),

$$R_{QPS}(T) \approx A\frac{R_Q^2}{R_N}\frac{L^2}{\xi^2(0)}\exp\left[-A\frac{R_Q}{R_N}\frac{L}{\xi(T)}\right], \tag{2}$$

where $R_Q \approx 6.45\ \text{k}\Omega$ is the quantum resistance. L is the NW length, A is a numerical parameter, and $F(T)$ is phase slip activation energy (Trezza et al. 2013). The results of the theoretical analysis are reported in Fig. 9 where the best-fit curves, which contain T_c, A, and L as adjustable parameters and which nicely reproduce the experimental data, are represented by solid lines. The dashed lines in Fig. 9 are obtained from Eq. 1 considering only the TAPS contribution to the resistance and disregarding the QPS term. These results show that the pronounced resistance tail exhibited by the two samples indeed originate from quantum phase slip processes. Moreover, since the theoretical models used to fit the experimental data were derived for an individual wire, the results of Fig. 9 show that the theory can reproduce the transition of NWs network with finite width and activation energy distribution. The

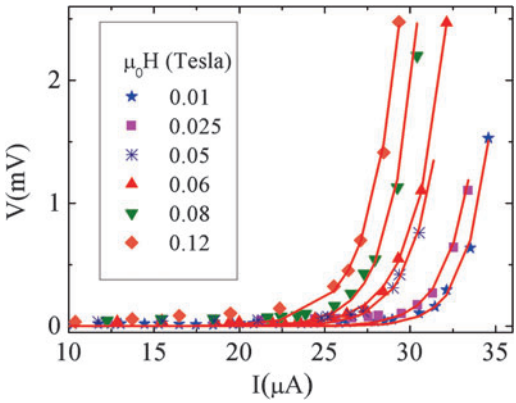

Fig. 10 Voltage–current characteristics measured at $T = 2.2$ K at different magnetic fields. Lines are the QPS fits to the data. Data are for the sample B

numbers for T_c, as obtained from the fitting procedure, were in reasonable agreement with the measured values. The values for L were close to 300 nm for sample A and 70 nm for sample B (Cirillo et al. 2012; Trezza et al. 2013). These numbers appear to be rather small if directly compared to the length of the Nb strip. However, this discrepancy could be explained considering that L is not a quantity that can be strictly defined for the network because, in a disordered system, it more likely represents a "percolation" length. Similar results related to the contribution of both TAPS and QPS to the resistive transition is reported also for Sn NWs grown *inside* the pores of porous anodic alumina templates with pore diameter smaller than 60 nm (Kline et al. 2006).

Generally, the NW networks grown *onto* a template have greater resolution patterning and are easier to grow by relatively simple vacuum deposition techniques compared to NW networks obtained depositing the material *inside* the template. In fact, to fabricate NW inside a pore having a diameter smaller than 70 nm, chemical or electrochemical methods should be used. Up to now, only soft superconducting metals, like Sn, Pb, Bi, and Ga, were successfully grown *inside* arrays of pores with that dimension (Kline et al. 2006; Charnaya et al. 1998). Information on the deposition *inside* the pores of refractory metals (Nb, Ti) and compounds (NbN, NbTiN) (which are most promising materials for the on-chip applications) is still lacking.

The role of quantum fluctuations at low temperature is further highlighted if $V(I)$ characteristics are measured as a function of the magnetic field. Some of them, measured for the sample B at T = 2.2 K and magnetic fields in the range 0.01–0.12 T, are shown in Fig. 10. The curves were fitted using the expressions valid if TAPS or QPS are responsible for the phase slippage. For thermal activation of phase slips, it is (Arutyunov et al. 2008; Golubev and Zaikin 2008)

$$V_{TAPS} = \frac{2\pi h}{e}\gamma_{TAPS}\sinh\left(\frac{hI}{4ek_BT}\right), \tag{3}$$

with $\gamma_{TAPS} \sim (R_{TAPS}/R_Q)(k_B T/h)$ (Golubev and Zaikin 2008). If quantum tunneling of phase slips takes place, V_{QPS} has a complicated expression which essentially gives for the $V(I)$ dependence a ~ sinh(I) behavior (Arutyunov et al. 2008). However, in the high-current (low temperature) limit, it simply reduces to (Arutyunov et al. 2008; Zaikin et al. 1997)

$$V_{QPS} \sim I^{2\mu-1} \tag{4}$$

with $\mu = R_Q/R_{qp}$. Here R_{qp} is a resistance of the order of R_n (Zaikin et al. 1997), which can be considered as a fitting parameter. The best fits to the $V(I)$ data, shown by solid lines in Fig. 10, were obtained using Eq. 4. The values extracted for the parameter R_{qp} depend on the magnetic field and are all lower than R_n, going from ~ 600 Ω at $\mu_0 H = 0.01$ T to ~ 800 Ω at $\mu_0 H = 0.14$ T. This result is consistent with the fact that, since R_{qp} represents the low-temperature residual resistance (Zgirski et al. 2008), it should tend to R_n when the applied magnetic field becomes larger. If the field is increased beyond 0.14 T, the best-fit curves do not satisfactorily reproduce the experimental data (Trezza et al. 2013).

If the average pore diameter in the PS template is further decreased, the coherence between NWs becomes stronger. This results in the oscillations of the transition $R(H)$ curves (Cirillo et al. 2014). In Fig. 11 we show the oscillatory field dependence of the $R(H)$ transition, measured at $T = 2.91$ K, for sample C ($d_{Nb} = 8.5$ nm)

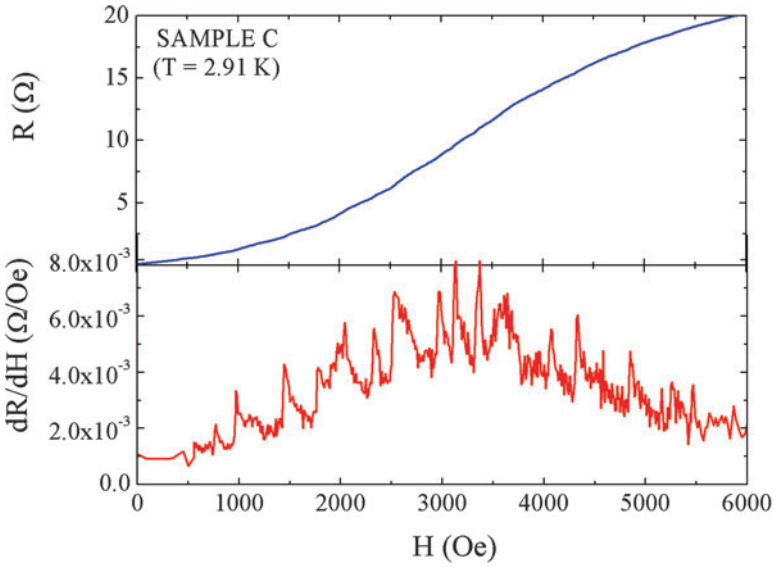

Fig. 11 The *top* (*bottom*) panel shows the MR transition, $R(H)$, (first MR derivative, $dR/dH(H)$) for sample C at $T = 2.91$ K

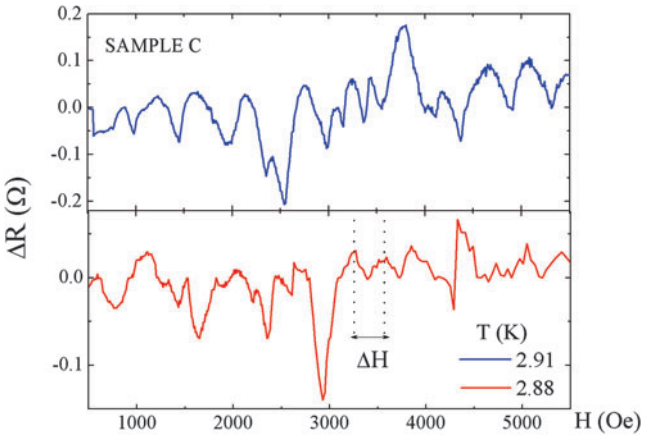

Fig. 12 ΔR data for sample C at two different temperatures. *Lines* indicate a selection of peak positions

sputtered on a PS template having $\varnothing \approx 10$ nm, $\Lambda \approx 40$ nm, and $w \approx 30$ nm. The effect is disclosed superimposing on the right scale the first $R(H)$ derivatives a function of the field, dR/dH, showing that the oscillations are present throughout the transition range, up to R_n. While the shape of the resistive transitions indicates the strong influence of fluctuations, the magnetoresistance (MR) oscillations are fingerprints of a coherent state and demonstrate the multiple connectedness of the sample. A simple explanation based on the Little-Parks effect must be excluded. Indeed, within the Little-Parks formalism, for the obtained period of oscillations, the average pore diameter should be as high as 300 nm, which is far from the value of $\varnothing$ for this sample (Cirillo et al. 2014). Thus, in order to better appreciate the oscillatory $R(H)$ dependence initially recognized in the dR/dH curves, a smooth background was subtracted from the original $R(H)$ curves. The resulting ΔR values are displayed in Fig. 12 for sample C at 2 different temperatures, $T = 2.88$ and 2.91 K. It is evident that the oscillatory behavior has a periodic or possibly a multiple periodic character, due to the presence of many possible current loops (Hansma and Kirtley 1974). Nevertheless, the largest periodicity, $\Delta H \approx 300$ Oe, which corresponds to the smallest area, is well detectable up to $H \approx 4000$ Oe.

The most plausible explanation of the observed periodicity of the $R(H)$ curves is based on the idea of nanowire quantum interference device (NQUID) (Hopkins et al. 2005; Pekker et al. 2005). In these works, authors considered two short NWs in a Dayem bridge configuration and modeled them as a pair of current-based Josephson junctions. The wires behave as 1D objects governed by TAPS processes, but due to the geometry of the system, constraints are imposed on the phase of the superconducting order parameter in the NQUID. Therefore, according to the model proposed by the authors, it results that the MR period of the device is determined not only by the flux concentrated to the area $2cb$ but also by the effective area $4cl$:

$$\Delta H = \left[\left(\frac{\Phi_0}{4cl} \right)^{-1} + \left(\frac{\Phi_0}{2cb} \right)^{-1} \right]^{-1}. \quad (5)$$

Here b is for length of the NW, $2c$ is the distance between NWs, and $2l$ is the width of two mesoscopic superconducting leads.

Conclusions

PS templates allow to fabricate macroscopically large and highly complex superconducting structures at low cost, quickly, and with an accuracy at the nanoscale level, which goes well beyond the up-to-date wet and dry lithographic technologies. The main features of such complex structures are the possibility to control the thermodynamic critical parameters of ultrathin superconducting films and to exhibit quantum coherence effects in arrays of multiply connected superconducting NWs. The interest of such novel devices is not only fundamental but also of applicative nature. In fact, their operation mimics those of a superconducting nanowire quantum interference detector with a proper spatial resolution capable of the detection of small spin systems, since the sensitivity to detect small magnetic fields scales with the NQUID loop radius (Granata et al. 2008). In this short review, we mainly concentrated on the results obtained on superconducting NWs and NW networks obtained by depositing *onto* porous templates. On the other hand, the properties of superconducting NWs grown *inside* porous silicon are less studied because the growth of NWs of refractory metals and compounds inside mesoscopic pores is a very complex task. This is a challenge that should be solved in the future.

References

Arutyunov KY, Golubev DS, Zaikin AD (2008) Superconductivity in one dimension. Phys Rep 464 (1/2):1–70

Astafiev OA, Ioffe LB, Kafanov S, Pashkin YA, Arutyunov KY, Shahar D, Cohen O, Tsai JS (2012) Coherent quantum phase slip. Nature 484(7394):355–358

Bisi O, Ossicini S, Pavesi L (2000) Porous silicon: a quantum sponge structure for silicon based optoelectronics. Surf Sci Rep 38(1–3):1–126

Bogomolov V, Yu K, Romanov S, Zhuravlev V (1993) Josephson properties of three-dimensional regular lattice of the weakly coupled nanoparticles. Phys C 208(3/4):371–384

Charnaya EV, Tien C, Lin KJ, Wur SC, Kumzerov YA (1998) Superconductivity in gallium in various confined geometries. Phys Rev B 58(1):467–472

Cirillo C, Trezza M, Chiarella F, Vecchione A, Bondarenko VP, Prischepa SL, Attanasio C (2012) Quantum phase slips in superconducting Nb nanowire networks deposited on self-assembled Si templates. Appl Phys Lett 101:172601 (1–5)

Cirillo C, Prischepa SL, Trezza M, Bondarenko VP, Attanasio (2014) Superconducting nanowire quantum interference device based on Nb ultrathin films deposited on self-assembled porous Si templates. Nanotechnology 25:425205 (1–9)

Cunin F (2014) Functional coatings of porous silicon. In: Canham L (ed) Handbook of porous silicon, 1st edn. Springer International Publishing, Switzerland pp 647–663

Giordano N (1990) Dissipation in a one-dimensional superconductor: evidence for macroscopic quantum tunneling. Phys Rev B 41(10):6350–6356
Golubev DS, Zaikin AD (2001) Quantum tunneling of the order parameter in superconducting nanowires. Phys Rev B 64(1):014504 (1–14)
Golubev DS, Zaikin AD (2008) Thermally activated phase slips in superconducting nanowires. Phys Rev B 78(14):144502 (1–8)
Graf MG, Huber TE, Huber CA (1992) Superconducting properties of indium in the restricted geometry of porous Vycor glass. Phys Rev B 45(6):3133–3136
Granata C, Esposito E, Vettoliere A, Petti L, Russo M (2008) An integrated superconductive magnetic nanosensor for high-sensitivity nanoscale applications. Nanotechnology 19 (27):275501
Hansma PK, Kirtley JR (1974) Two-dimensional arrays of Josephson weak links. J Appl Phys 45 (9):4016–4024
Hongisto TT, Zorin AB (2012) Single-charge transistor based on the charge-phase duality of a superconducting nanowire circuit. Phys Rev Lett 108(9):097001 (1–5)
Hopkins D, Pekker D, Goldbart PM, Bezryadin A (2005) Quantum interference device made by DNA templating of superconducting nanowires. Science 308(5729):1762–1765
Kline TR, Tian M, Wang J, Sen J, Chan MWH, Mallouk TE (2006) Template-grown metal nanowires. Inorg Chem 45(19):7555–7565
Lau CN, Markovic N, Bockrath M, Bezryadin A, Tinkham M (2001) Quantum phase slips in superconducting nanowires. Phys Rev Lett 87(21):217003 (1–4)
Lehtinen JS, Sajavaara T, Arutyunov KY, Presnjakov MY, Vasiliev AL (2012) Evidence of quantum phase slip effect in titanium nanowires. Phys Rev B 85(9):094508 (1–7)
Luo Q, Zeng XQ, Miszczak ME, Ziao ZL, Pearson J, Xu T, Kwok WK (2012) Phase slippage driven dissipation and high-field Little-Parks effect in superconducting MoGe nanowire networks formed on nanoporous substrates. Phys Rev B 85(17):174513 (1–7)
Mooij JE, Harmans CJPM (2005) Phase-slip flux qubits. New J Phys 7:219
Mooij JE, Nazarov YV (2006) Superconducting nanowires as quantum phase-slip junctions. Nat Phys 2(3):169–172
Moshchalkov VV, Baert M, Metlushko VV, Rosseel E, Van Bael MJ, Temst K, Bruynseraede Y, Jonckheere R (1998) Pinning by antidote lattice: the problem of the optimum antidote size. Phys Rev B 57:3615–3622
Ogata YH, Fukami K (2014) Porous silicon and electrochemical deposition. In: Canham L (ed) Handbook of porous silicon,1st edn. Springer International Publishing, Switzerland pp 629–637
Patel U, Xiao ZL, Hua J, Xu T, Rosenmann D, Novosad V, Pearson J, Welp U, Kwok WK, Crabtree GB (2007) Origin of the matching effect in a superconducting film with a hole array. Phys Rev B 76(2):020508(R)(1–4)
Pekker D, Bezryadin A, Hopkins DS, Goldbart PM (2005) Operation of a superconducting nanowire quantum interference device with mesoscopic leads. Phys Rev B 72(10):104517 (1–18)
Prischepa SL, Lynkov LM, Lykov AN, Dedyu VI (1994) Porous anodic Al_2O_3 layers for superconducting films. Cryogenics 34:851–853
Remeika M, Bezryadin A (2005) Sub-10 nanometer fabrication: molecular templating, electron-beam sculpting and crystallization of metallic nanowires. Nanotechnology 16(8):1172–1176
Schmidt VV (1997) The physics of superconductors: introduction to fundamentals and applications (eds: Müller P, Ustinov AV). Springer, Berlin, 206 p
Tettamanzi GC, Pakes CI, Potenza A, Rubanov S, Marrows CH, Prawer S (2009) Superconducting transition Nb nanowires fabricated using focused ion beam. Nanotechnology 20(46):465302
Tian M, Wang J, Kurtz JS, Liu Y, Chan MHW, Mayer TS, Mallouk TE (2005) Dissipation in quasi-one-dimensional single-crystal Sn nanowires. Phys Rev B 71(10):104521 (1–7)

Trezza M, Prischepa SL, Cirillo C, Fittipaldi R, Sarno M, Sannino D, Ciambelli P, Hesselberth MBS, Lazarouk SK, Dolbik AV, Borisenko VE, Attanasio C (2008) Superconducting properties of Nb thin films deposited on porous silicon templates. J Appl Phys 104(8):083917 (1–7)

Trezza M, Cirillo C, Prischepa SL, Attanasio C (2009) Evidence of fractional matching states in nanoperforated Nb thin film grown on porous silicon. Europhys Lett 88:57006 (1–6)

Trezza M, Cirillo C, Sabatino P, Carapella, Prischepa SL, Attanasio (2013) Nonlinear current–voltage characteristics due to quantum tunneling of phase slips in superconducting Nb nanowire networks. Appl Phys Lett 103(25):252601 (1–4)

Vinckx W, Vanacken J, Moshchalkov VV, Mátéfi-Tempfi S, Mátéfi-Tempfi M, Michotte S, Piraux L (2006) Vortex pinning in superconducting Nb thin films deposited on nanoporous alumina templates. Eur Phys J B 53(2):199–203

Vinckx W, Vanacken J, Moshchalkov VV, Mátéfi-Tempfi S, Mátéfi-Tempfi M, Michotte S, Piraux L, Ye X (2007) High field matching effects in superconducting Nb porous arrays catalyzed from anodic alumina templates. Phys C 459(1–2):5–10

Webster CH, Fenton JC, Hongisto TT, Giblin SP, Zorin AB, Warburton PA (2013) NbSi nanowire quantum phase-slip circuits: dc supercurrent blockage, microwave measurements and thermal analysis. Phys Rev B 87(14):144510 (1–12)

Welp U, Xiao ZL, Jiang JS, Vlasko-Vlasov VK, Bader SD, Crabtree GW, Liang J, Chik H, Xu JM (2002) Superconducting transition and vortex pinning in Nb films patterned with nanoscale hole arrays. Phys Rev B 66(21):212507 (1–11)

Xia Y, Rogers JA, Paul KE, Whitesides GM (1999) Unconventional methods for fabricating and patterning nanostructures. Chem Rev 99(7):1823–1848

Zaikin AD, Golubev DS, van Otterlo A, Zimányi GT (1997) Quantum phase slips and transport in ultrathin superconducting wires. Phys Rev Lett 78(8):1552–1555

Zgirski M, Riikonen KP, Touboltsev V, Arutyunov KY (2008) Quantum fluctuations in ultranarrow superconducting aluminum nanowires. Phys Rev B 77(5):054508 (1–6)